EFFECTS OF COBALT AND CHROMIUM IONS ON OXIDATIVE STRESS AND ENERGY METABOLISM IN MACROPHAGES *IN VITRO*

Zeina Salloum[1], Eric A. Lehoux[2],

Mary-Ellen Harper[1], Isabelle Catelas[1,2,3]

[1] Department of Biochemistry, Microbiology and Immunology, Faculty of Medicine, University of Ottawa, 451 Smyth Road, Ottawa, ON, Canada, K1H 8M5

[2] Department of Mechanical Engineering, Faculty of Engineering, University of Ottawa, 161 Louis Pasteur, Ottawa, ON, Canada, K1N 6N5

[3] Department of Surgery, University of Ottawa, The Ottawa Hospital–General Campus, 501 Smyth Road, Ottawa, ON, Canada K1H 8L6

Running Title: Oxidative stress and energy metabolism in macrophages

Contribution statement:

All authors have contributed to the research design, analysis, interpretation of the data, and writing of the manuscript. All authors have read and approved the submitted manuscript.

Correspondence should be sent to:
Isabelle Catelas, Ph.D., P.Eng
Department of Mechanical Engineering
Phone: +1-613-562-5800, Ext. 8589
Fax: +1-613-562-5177
E-mails: icatelas@uottawa.ca / icatelas@hotmail.com

ABSTRACT

Cobalt and chromium ions released from cobalt-chromium-molybdenum (CoCrMo)-based implants are a potential health concern, especially since both ions have been shown to induce oxidative stress in macrophages, the predominant immune cells in periprosthetic tissues. Other transition metal ions (Cd^{2+}, Ni^{2+}) have been reported to inhibit the activity of mitochondrial enzymes in the electron transport chain. However, the effects of Co and Cr ions on the energy metabolism of macrophages remain largely unknown. The objective of the present study was to analyze the effects of Co^{2+} and Cr^{3+} on oxidative stress and energy metabolism in macrophages *in vitro*. RAW 264.7 murine macrophages were exposed to 6-18 ppm Co^{2+} or 50-150 ppm Cr^{3+}. Results showed a significant increase in two markers of oxidative stress, reactive oxygen species (ROS) level and protein carbonyl content, with increasing concentrations of Co^{2+}, but not Cr^{3+}. In addition, oxygen consumption rates (OCR; measured using an extracellular flux analyzer) showed significant decreases in both mitochondrial respiration and non-mitochondrial oxygen consumption with increasing concentrations of Co^{2+}, but not Cr^{3+}. OCR results further showed that Co^{2+}, but not Cr^{3+}, induced mitochondrial dysfunction, including a decrease in oxidative phosphorylation capacity. Overall, this study suggests that mitochondrial dysfunction may contribute to Co^{2+}-induced oxidative stress in macrophages, and thereby to the inflammatory response observed in periprosthetic tissues.

Keywords: metal implants, metal ions, oxidative stress, energy metabolism, macrophages

INTRODUCTION

Cobalt-chromium-molybdenum (CoCrMo) alloys are used extensively in orthopaedic applications.[1] However, these alloys can undergo wear and corrosion *in vivo*, leading to the release of Co and Cr ions, which are a potential health concern.[2-4] Indeed, clinical studies have shown elevated concentrations of Co and Cr ions in the blood, serum, and synovial fluid of patients with a CoCrMo joint implant associated with adverse soft tissue reactions.[5-7] Nevertheless, the adverse effects of Co and Cr ions on cellular physiology remain largely unknown.

Both Co^{2+} and Cr^{3+} have been shown to induce adverse effects on cellular components including proteins, lipids, and nucleic acids.[8] For example, Petit et al.[9] reported that these metal ions induced an increase in protein carbonyl content (a measure of oxidative damage and a common marker for oxidative stress[10]) in U937 monocytes. In addition, Scharf et al.[11] reported a strong positive correlation between protein carbonyl content in periprosthetic tissues and the amount of Co and Cr present in these tissues. High levels of oxidative stress induced by Co^{2+} and Cr^{3+} may therefore contribute to adverse reactions in periprosthetic tissues, such as necrosis and soft tissue masses known as pseudotumors,[11] which often lead to implant failure.[12]

Oxidative stress (defined as 'an imbalance between oxidants and antioxidants in favor of the oxidants, leading to a disruption of redox [reduction-oxidation] signaling and control and/or molecular damage'[13]) has been linked to various disease states.[14] Intracellular sources of reactive oxygen species (ROS) include enzymatic systems such as nicotinamide adenine dinucleotide phosphate (NADPH) oxidase (which produces superoxide anions) and organelles such as mitochondria, the endoplasmic reticulum (under stress), and peroxisomes.[15] NADPH oxidase protein complexes, located in the plasma membrane, are particularly important for ROS production in certain cell types, including macrophages.[15] Overall, in most cell types, mitochondria are thought

to be the major ROS-producing organelles because a high number of redox reactions occur therein. Major sites of mitochondrial ROS production include complexes I and III of the electron transport chain (ETC), and other redox enzymes such as pyruvate dehydrogenase.[16,17] The ETC, located in the mitochondrial inner membrane, is comprised of a series of four redox carrier complexes: nicotinamide adenine dinucleotide dehydrogenase, also known as NADH-ubiquinone oxidoreductase (complex I); succinate dehydrogenase (complex II); cytochrome c reductase (complex III); and cytochrome oxidase (complex IV). The ETC is coupled to oxidative phosphorylation through a proton gradient that is used by the F_0F_1 ATP synthase complex to produce ATP.

Redox-active metals play an essential role in the regulation of both mitochondrial and non-mitochondrial protein complexes.[18,19] Interestingly, it has been shown that Co^{2+} and Cu^{2+} can compete with Fe^{2+} for Fe binding sites in iron-sulfur clusters (which play a central role in the ETC), resulting in their mismetallation.[20] Since Co^{2+} and Cu^{2+} (as well as Ni^{2+}) rank higher than Fe^{2+} on the Irving-Williams Series, they can form more stable complexes than Fe^{2+}.[21] Furthermore, $Cd^{2+}$and Ni^{2+} have been shown to inhibit the activity of mitochondrial enzymes in the ETC[22,23] and induce mitochondrial ROS production.[22,24]

Finally, *in vitro* studies have shown that both Co^{2+} and Cr^{3+} can activate the production of bone-resorbing cytokines through the activation of redox-dependent mechanisms[25] and induce an inflammatory response in macrophages,[25,26] the predominant immune cells in periprosthetic tissues.[27,28] The bioenergetic demands of such an inflammatory response require a stepwise adaptation of cellular energy metabolism.[29] However, the effects of Co^{2+} and Cr^{3+} on the energy metabolism of macrophages remain largely unknown. Therefore, the objective of the present study was to analyze the effects of Co^{2+} and Cr^{3+} on oxidative stress and energy metabolism in macrophages *in vitro*.

MATERIALS AND METHODS

Unless otherwise specified, water was reagent grade (ASTM Type I).

Metal ions

Stock solutions of Co^{2+} and Cr^{3+} were prepared fresh, as previously described.[30] Briefly, $CoCl_2$•$6H_2O$ (99.5% purity; Fisher Scientific, Waltham, MA) and $CrCl_3$•$6H_2O$ (100.8% purity; Sigma, St Louis, MO) were dissolved in cell culture-grade water (Lonza, Walkersville, MD) and the solutions were sterilized by filtration through 0.2-μm pore size cellulose acetate syringe filters (VWR, Mississauga, ON). Sterilized solutions of Co^{2+} and Cr^{3+}contained ≤ 0.01 endotoxin unit (EU)/mL, as determined using a chromogenic *Limulus* amebocyte lysate assay (GenScript, Piscataway, NJ).

Cells

The RAW 264.7 murine macrophage cell line (American Type Collection Culture [ATCC]; Manasas, VA) was maintained at 37ºC in a humidified atmosphere of 95% air and 5% CO_2 in 100-mm diameter tissue culture-treated polystyrene dishes (Greiner Bio-One; Monroe, NC). The cells were cultured in Dulbecco's modified Eagle medium (DMEM)-based growth medium (DMEM [Wisent; St. Bruno, QC] supplemented with 10% [v/v] qualified-grade heat-inactivated fetal bovine serum [FBS; Gibco, Carlsbad, CA]), and passaged ≤ 10 times from the working culture received from ATCC. For experiments (and routine subculture), cells were detached by pipetting using a Class A volumetric glass pipette (Sibata Scientific Technology, Soka, Japan) and resuspended in the above growth medium to 0.5×10^6 cells/mL, unless otherwise specified.

Cell mortality

Six-well tissue culture-treated polystyrene multiwell plates (Greiner Bio-One) were seeded with 2 mL of cell suspension (0.5×10^6 cells/mL) per well and incubated 2-3 hours under cell culture conditions to allow cell attachment. At the end of the incubation, the culture supernatants were replaced with 2 mL of growth medium containing Co^{2+} (6 to 24 ppm), Cr^{3+} (50 to 250 ppm), or no addition (negative control), and the cells were incubated an additional 24 hours.

At the end of the incubation, cells were detached by gentle pipetting using a 1-mL manual single-channel pipette (Mettler Toledo, Oakland, CA) and the cell suspensions were transferred into 5-mL untreated polystyrene culture tubes (Corning, Corning, NY). Cell mortality was analyzed by dye-exclusion hemocytometry under phase contrast microscopy using trypan blue (0.04% [w/v] final concentration; Sigma-Aldrich) and an improved Neubauer hemocytometer (Hausser Scientific, Horsham, PA).

Cytosolic reactive oxidative species (ROS)

Ninety-six-well tissue culture-treated black-wall polystyrene multiwell plates with a clear flat bottom (Greiner Bio-One) were seeded with 200 µL of cell suspension (0.5×10^6 cells/mL) per well and incubated 2-3 hours under cell culture conditions to allow cell attachment. At the end of the incubation, the culture supernatants were discarded and the cells in each well were washed twice with 100 µL of phenol red-free Hank's balanced salt solution (HBSS; Lonza) to remove traces of phenol red and FBS. Cytosolic ROS level was measured using a cell-based fluorescence assay (OxiSelect™ Intracellular ROS assay kit; Cell Biolabs, San Diego, CA) as per the manufacturer's instructions. Briefly, cells were incubated 1 hour at 37°C with 100 µM 2′,7′-dichlorodihydrofluorescein diacetate (a cell-permeant fluorogenic probe) prepared in phenol red-free low glucose DMEM (Sigma-Aldrich) supplemented with 1.5 g/L of cell-culture grade

$NaHCO_3$ (Sigma-Aldrich) and an additional 3.5 g/L of cell-culture grade D-glucose (Sigma-Aldrich) to replicate the formulation of the DMEM used to culture the cells. The cells were then washed two more times with phenol red-free HBSS and incubated 6 hours in 100 µL of phenol red-free DMEM (Sigma-Aldrich) supplemented with 10 % (v/v) heat-inactivated FBS, $NaHCO_3$ and D-glucose as above, and containing Co^{2+} (6 to 18 ppm), Cr^{3+} (50 to 150 ppm), H_2O_2 (100 µM; positive control; data not shown) or no addition (negative control). At the end of the incubation, dichlorofluorescein (DCF) fluorescence was measured with a hybrid microplate reader (Synergy™ 4; Biotek, Winooski, VT) using excitation and emission wavelengths of 480 and 530 nm, respectively.

Protein carbonylation

One hundred-mm diameter tissue culture-treated dishes (Greiner Bio-One) were seeded with 12 mL of cell suspension (0.5×10^6 cells/mL) per dish and incubated 2-3 hours under cell culture conditions to allow cell attachment. At the end of the incubation, the culture supernatants were replaced with 12 mL of growth medium containing Co^{2+} (6 to 18 ppm), Cr^{3+} (50 to 150 ppm), or no addition (negative control), and the cells were incubated an additional 24 hours.

At the end of the 24-hour incubation, the cells were washed twice with ice-cold Dulbecco's phosphate-buffered saline (DPBS) without Ca^{2+} and Mg^{2+} (Sigma-Aldrich) and detached carefully, using a 2-cm chiseled-edge polypropylene cell lifter (Fisher Scientific), in 1 mL (per dish) of ice-cold lysis buffer (50 mM tris [Sigma-Aldrich]; 150 mM NaCl [Fisher Scientific]; 1 mM ethylenediaminetetraacetic acid [EDTA; Fisher Scientific], pH 7.4) supplemented with an EDTA-free protease inhibitor cocktail (Roche Diagnostics; Indianapolis, IN) as per the manufacturer's instructions. The detached cells (in ca. 1-mL aliquots) were lysed by nitrogen cavitation (see Discussion) following a 5-min exposure to a pressure of 1250 psi inside a 45-mL capacity cell-

disruption vessel (model number 4639; Parr Instrument, Moline, IL). Insoluble cellular material was removed from the lysates by centrifugation (21,000 × *g* for 30 min at 4°C). Supernatants were concentrated by centrifugal filtration (3,500 × *g* for 30 min at 4°C) using 4-mL capacity 10-kDa molecular weight cut-off low-binding regenerated cellulose filters (Millipore, Billerica, MA). Aliquots of the concentrated samples, in argon-filled 0.5-mL polypropylene cryovials (Simport; Beloeil, QC), were frozen and stored in liquid nitrogen for future protein carbonyl content analysis. Protein determination was performed using the bicinchoninic acid colorimetric assay with bovine serum albumin (BSA) as the protein standard (Thermo Scientific, Rockford, IL). Absorbance was measured at a wavelength of 562 nm using a hybrid microplate reader (Biotek).

Protein carbonyl content was quantified by immunochemical detection after derivatization with 2,4-dinitrophenylhydrazine (DNPH) as described by Wehr et al.[31], with minor modifications. Cell lysate proteins oxidized by exposure to $FeCl_3$ and ascorbate[32] (which together act as a ROS-generating system[33]) were used as a positive control (data not shown). Briefly, samples (3 µg protein/µL) were mixed with one volume of sodium dodecyl sulfate (SDS) solution (20% [w/v]; Fisher Scientific) and two volumes of DNPH solution (20 mM [Sigma-Aldrich] in 10% (v/v) trifluoroacetic acid [Sigma-Aldrich]), then incubated 15 min at room temperature. The incubation was terminated by adding two volumes of neutralization solution (1.5 M tris, 22.5% [v/v] glycerol [Sigma-Aldrich]). Aliquots (3 µg protein) of the derivatized samples were mixed with sample loading buffer (LI-COR, Lincoln, NE), as per the manufacturer's instructions (except that the final loading buffer concentration was 0.5X and, as recommended by Wang et al.[34], the reducing agent was omitted), and analyzed by SDS-polyacrylamide gel electrophoresis (PAGE) using precast mini-format tris-glycine gradient (8-16%) gels (Bio-Rad; Hercules, CA). Pre-stained (visible and near-infrared) protein molecular weight standards (LI-COR) and 2,4-dinitrophenyl (DNP)-derivatized protein molecular weight standards (OxyBlot® Protein Oxidation Detection Kit;

Millipore) were used (note: the molecular weights provided by the manufacturer for the DNP-derivatized standards are those of the underivatized proteins and are therefore likely underestimated). Two identical gels were run in parallel: one was used for western blotting (this gel was truncated above the 260 kDa molecular weight mark prior to electrotransfer to avoid gel compression artifacts), and the other was stained with Coomassie Brilliant Blue R-250 dye (Bio-Rad). For western blotting, proteins were electrotransferred onto a 0.45-µm pore size fluorescent-grade polyvinylidene fluoride (PVDF) membrane (Immobilon-FL; Millipore). The membrane was air-dried overnight, reversibly stained for total protein with acid blue (REVERT™ total protein stain; LI-COR) as per the manufacturer's instructions, and imaged at 700 nm using a near-infrared fluorescence/chemiluminescence imaging system (Odyssey® Fc; LI-COR). Immunodetection was performed using a rabbit anti-DNP antibody as the primary antibody and a goat anti-rabbit horseradish peroxidase (HRP)-conjugated antibody as the secondary antibody (OxyBlot® Protein Oxidation Detection Kit; Millipore), as per the manufacturer's instructions. DPBS containing 0.1% (v/v) polysorbate 20 (Fisher Scientific) and 1% (w/v) BSA was used as the blocking and antibody dilution buffer. Chemiluminescence detection was performed using chemiluminescent HRP substrate (Millipore) as per the manufacturer's instructions, and the blots were imaged using a near-infrared fluorescence/chemiluminescence imaging system (LI-COR). Chemiluminescence intensity was normalized to protein content determined by acid-blue staining. Both acid-blue staining and chemiluminescence were analyzed by densitometry using Image Studio™ software v.2.0 (LI-COR). No chemiluminescence was detected when DPNH was omitted from the derivatization step, thereby confirming the specificity of the detection system for the DNP moiety of the derivatized proteins (data not shown).

Cellular oxygen consumption

Cellular oxygen consumption rates (OCR) were measured using an extracellular flux analyzer (Seahorse XF96e; Agilent Technologies, Santa Clara, CA). Briefly, the cartridge sensors were incubated overnight at 37°C in a hydration/calibration solution (XF Calibrant; Agilent Technologies). Specially designed polystyrene tissue culture-treated 96-well microplates with a clear flat bottom (Seahorse XF96 V3 PS Cell Culture Microplates; Agilent Technologies) were then seeded with 80 µL of cell suspension (1.0×10^6 cells/mL) per well and incubated 2-3 hours under cell culture conditions to allow cell attachment.

At the end of the incubation, the culture supernatants were replaced with growth medium containing Co^{2+} (6 to 18 ppm), Cr^{3+} (50 to 150 ppm), no metal ions (negative control), or lipopolysaccharide (LPS) from *E. coli* O55:B05 (1 µg/mL; Sigma-Aldrich; positive control [data not shown]). The cells were incubated 6 hours under cell culture conditions, then washed and incubated 45 min at 37°C in base medium (phenol red-free low glucose DMEM [Sigma-Aldrich] supplemented with 3.5 g/L of cell-culture grade D-glucose [Sigma-Aldrich]). OCR were measured to assess resting respiration, then ATP production-dependent respiration, maximal respiration, and non-mitochondrial oxygen consumption, after sequential injections of oligomycin (an ATP synthase inhibitor) at 1 µM (final concentration), carbonyl cyanide *m*-chlorophenyl hydrazone (an ionophore acting as a proton uncoupler) at 2 µM, and rotenone and antimycin A (complex I and complex III inhibitors, respectively) at 0.5 µM. Spare respiratory capacity, a measure of the ability of cells to respond to increased energy demand, was calculated by subtracting resting respiration from maximal respiration. ATP production-dependent respiration was calculated by subtracting the lowest OCR after oligomycin injection from resting OCR. Proton leak, represented by basal respiration (i.e., mitochondrial respiration that is not coupled to ATP production), was calculated by subtracting the OCR corresponding to non-mitochondrial oxygen consumption from the lowest

OCR after oligomycin injection. Non-mitochondrial oxygen consumption was subtracted from the reported resting respiration, maximal respiration, spare respiratory capacity, and ATP production-dependent respiration. For each parameter, OCR measurements were performed 3 times at 6-min intervals. All OCR measurements were corrected for the OCR of cell-free wells containing only medium. Upon completion of the OCR measurements, the cells were washed once with PBS and lysed in 1M NaOH (40 μL/well). The lysates were kept at 4°C for up to 24 hours, and protein determination was performed using the Bradford colorimetric assay with BSA as the standard protein (Thermo Scientific). Absorbance was measured at a wavelength of 595 nm using a hybrid microplate reader (Biotek).

Statistical analysis

Statistical analysis was performed using IBM SPSS Statistics software for Windows, version 24.0 (IBM, Armonk, NY). The data were assumed to be normally distributed and Levene's test was used to determine if the assumption of homogeneity of variance was met. When met, a two-way analysis of variance (ANOVA) was used for group-wise comparisons followed by Tukey-Kramer post-hoc tests. When unmet, a Welch ANOVA was performed followed by Games-Howell post-hoc tests. $p<0.05$ was considered significant. Effect sizes are presented as Cohen's d with 95% confidence intervals (CI). Data are presented as means ± standard errors of the means (SEM).

RESULTS

Effects of Co^{2+} and Cr^{3+} on macrophage mortality

Results revealed a Co^{2+} concentration-dependent increase in the percentage of dead macrophages of up to 33% with 24 ppm Co^{2+} (d=2.5, 95% CI [0.3, 4.6]; p<0.001, Figure 1A), relative to the negative control (cells unexposed to Co^{2+} or Cr^{3+}). Cr^{3+} also induced a concentration-dependent increase in the percentage of dead cells of up to 27% with 250 ppm (d=5.2, 95% CI [1.9, 8.6]; p<0.001, Figure 1B), relative to the negative control. It should be noted that since the percentage of dead cells is calculated based on the total number of cells (live + dead) present at the end of the 24-hour exposure, disintegrated cells are excluded from this percentage.

The total number of macrophages (live + dead) exposed to Co^{2+} and Cr^{3+} increased due to proliferation, except with 18 and 24 ppm Co^{2+} where death resulting in cellular disintegration decreased the total number of cells below the initial 1×10^6. However, the total number of macrophages was lower after exposure to Co^{2+}, relative to the negative control, at all the concentrations tested (up to 87% lower with 24 ppm Co^{2+}; d=15.1, 95% CI [6.4, 23.8]; p<0.001, Figure 1C). In contrast, after exposure to Cr^{3+}, the total number of macrophages was lower, relative to the negative control, only at the highest concentration tested (44% lower with 250 ppm Cr^{3+}; d=5.2, 95% CI [1.8, 8.5]; p<0.001, Figure 1D).

Effects of Co^{2+} and Cr^{3+} on oxidative stress in macrophages

Results revealed a Co^{2+} concentration-dependent increase in cytosolic ROS level of up to 520% with 18 ppm Co^{2+} (d=10.2, 95% CI [5.9, 14.4]; p<0.001; Figure 2A), relative to the negative control, after a 6-hour exposure. In contrast, Cr^{3+} did not induce any significant changes in ROS level (Figure 2B).

Results also revealed a Co^{2+} concentration-dependent increase in protein carbonyl content of 31% and 86% with 12 ppm and 18 ppm Co^{2+}, respectively (d=8.7, 95% CI [3.5, 13.9] and d=3.8, 95% CI [1.1, 6.5], respectively; p<0.05; Figure 3A), relative to the negative control, after a 24-hour

exposure. In contrast, Cr^{3+} did not induce any significant changes in protein carbonyl content (Figure 3B).

Effects of Co^{2+} and Cr^{3+} on macrophage oxygen consumption rates

Results revealed a Co^{2+} concentration-dependent decrease in resting respiration of up to 26% with 18 ppm Co^{2+} (d=3.8, 95% CI [2.8, 4.7]; p<0.001; Figure 4A), relative to the negative control. Similarly, a decrease was observed in ATP production-dependent respiration (up to 24%; d=2.9, 95% CI [2.1, 3.8]), maximal respiration (up to 43%; d=4.4, 95% CI [3.3, 5.4]), and spare respiratory capacity (up to 60%; d=4.0, 95% CI [3.0, 5.0]) (p<0.001 in all cases; Figure 4A). A decrease was also observed in non-mitochondrial oxygen consumption (up to 21%; d=1.1, 95% CI [0.4, 1.7]; p<0.001; Figure 4B), and in proton leak with all Co^{2+} concentrations (up to 33%; d=5.3, 95% CI [4.1, 6.5]; p<0.001; Figure 4C).

In contrast, Cr^{3+} did not induce any significant changes in OCR except for proton leak, which decreased only with 100 ppm Cr^{3+} (d=4.2, 95% CI [3.2, 5.2]; p<0.001; Figure 5C), relative to the negative control.

DISCUSSION

The present study analyzed the effects of Co^{2+} and Cr^{3+} on oxidative stress and energy metabolism in macrophages, the predominant immune cells in periprosthetic tissues.[27,28] To the best of our knowledge, this is the first study to examine the effects of these metal ions on mitochondrial respiration parameters in cells and on oxidative stress in the context of mitochondrial dysfunction. Results showed that Co^{2+}, but not Cr^{3+}, induced ROS production and protein carbonylation, suggesting that Co^{2+} may be inducing oxidative stress through ROS. Results also showed that Co^{2+}, but not Cr^{3+}, adversely affected mitochondrial function in the macrophages.

The effects of Co^{2+} and Cr^{3+} were studied because Co and Cr are the primary components of CoCrMo alloys that are used extensively in orthopaedic applications. Co exists in two common oxidation states (+2 and +3). However, Co^{2+} were used in the present study because Co^{3+} are rapidly reduced to Co^{2+} in aqueous environments.[30] Similarly, Cr exists in two common oxidation states (+3 and +6), but Cr^{3+} were used in the present study because Cr^{6+} are rapidly reduced to Cr^{3+} under physiological conditions.[30] The ranges of Co^{2+} and Cr^{3+} concentrations used in the present study were based on: 1) previous studies analyzing the effects of Co^{2+} and Cr^{3+} on oxidative stress and inflammatory cytokine release from macrophages *in vitro*[9,25,26,35,36]; 2) the assumption that the concentration of these ions is higher in periprosthetic tissues than in body fluids where their concentrations are in the ppb range; and 3) the consideration that macrophage stimulation probably requires higher concentrations of a stimulating agent *in vitro* than it does *in vivo,* where cells are exposed to multiple stimulating factors simultaneously[26,36]. The RAW 264.7 murine macrophage cell line was used because it is a common model for *in vitro* studies of molecular pathways activated by implant wear particles or metal ions,[37-39] and of oxidative stress and mitochondrial function (e.g., Badding et al.[40]). Immortalized cells, as opposed to primary cells, were selected to avoid potential inter-donor variability. Limitations of the RAW 264.7 macrophage model include its murine origin,[41] as well as higher metabolic rates and OCR than primary murine macrophages.[42]

Mortality analysis showed a Co^{2+} concentration-dependent increase in the percentage of dead cells and lower total numbers of cells (live + dead) after a 24-hour exposure to Co^{2+}, at all the concentrations analyzed. The lower total numbers of cells were due to a concentration-dependent reduction in cell proliferation (as evidenced by a decrease in the proportion of actively dividing cells, as determined by fluorescence microscopy using Hoechst 33342 DNA staining; data not shown), as well as death resulting in cellular disintegration. In contrast to the results obtained with Co^{2+}, exposure to Cr^{3+} only increased the percentage of dead cells at the highest concentration

analyzed and the total number of cells was lower only at that concentration. Overall, these results reflect the greater cytotoxicity of Co^{2+}, relative to Cr^{3+}, in agreement with previous macrophage studies.[43-45]

The effects of Co^{2+} and Cr^{3+} on oxidative stress were analyzed through measurements of cytosolic ROS level and total protein carbonyl content. In macrophages, elevated concentrations of ROS (which are by-products of oxidative metabolism) can induce an inflammatory response through redox signalling,[46,47] and possibly lead to oxidative damage of cellular components and consequent impairment of cellular functions.[46] Reversible and irreversible oxidative modification of proteins by ROS occur during redox signaling and as a consequence of acute or chronic oxidative stress.[31] Since protein carbonylation occurs in many of these modifications, it is a standard marker for oxidative stress.[31] Overall, the results showed that Co^{2+}, but not Cr^{3+}, increased ROS levels by up to 520% and protein carbonyl content by up to 86%. By comparison, the exposure of RAW 264.7 macrophages to phorbol 12-myristate 13-acetate (PMA), a potent inducer of ROS production via NAPDH oxidase, has been reported to increase ROS production by up to ca. 1,200% at peak oxidative burst, and protein carbonyl content by up to ca. 30% approximately 25 min post-peak oxidative burst.[48] However, the magnitude of changes in ROS levels in the cells exposed to Co^{2+} should be interpreted cautiously because of the technical challenges presented by the detection of intracellular ROS.[49] Notwithstanding, the results of the present study suggest that exposure to Co^{2+} can cause a substantial increase in oxidative stress in macrophages by inducing ROS production. The mechanisms by which Co^{2+} induce ROS production in macrophages remain unclear. One of the mechanisms may involve Fenton-like reactions where intracellularly generated hydrogen peroxide (normally decomposed by catalase into water and oxygen) reacts with Co^{2+} to produce highly reactive hydroxyl radicals.[11] Excessive production of these radicals can overwhelm cellular antioxidant systems thereby causing oxidative stress.[50] *In vivo* exposure to Co^{2+} for 24 hours has

also been reported to decrease the activity of superoxide dismutase and catalase, two antioxidant enzymes playing a prominent role in the neutralization of ROS.[51] Other mechanisms by which Co^{2+} induce ROS production in macrophages may involve the ETC and NADH oxidase. As previously mentioned, in the absence of exogenous metal ions, cellular ROS production originates primarily from mitochondria and the plasma membrane where NADH oxidase complexes are located.

In the present study, the analysis of oxygen consumption showed significant decreases in mitochondrial respiration with increasing Co^{2+} concentrations, suggesting that Co^{2+} induce mitochondrial dysfunction and affect overall cellular energy metabolism. Specifically, results showed that Co^{2+}, but not Cr^{3+}, decreased resting respiration by up to 26%, ATP production-dependent respiration by up to 24%, and maximal respiration by up to 43%. By comparison, the polarization of naïve murine bone marrow-derived macrophages (BMDM) to the inflammatory (M1) phenotype by LPS and interferon-γ has been reported to decrease these respiration parameters by ca. 60%, 65%, and 85%, respectively.[52] The effects of Co^{2+} on the mitochondrial respiration parameters are therefore substantial and consistent with dysfunctional oxidative phosphorylation. A Co^{2+}-induced decrease in the capacity of mitochondria to produce ATP may thus have a significant impact on overall cellular energy metabolism and, as discussed below, may lead to the activation of mechanisms that help maintain cellular energy homeostasis.

The effects of Co^{2+} on mitochondrial respiration parameters may be due to interactions with pathways involved in the regulation of energy metabolism and/or mitochondrial components, including the ETC located in the mitochondrial inner membrane. ETC complexes I, II, and III contain iron-sulfur clusters and, as previously mentioned, Co^{2+} can cause mismetallation of these clusters by competing with Fe^{2+} for Fe binding sites.[20] This mismetallation may lead to ETC dysfunction and cause the release of Fe ions into the intracellular environment. The released Fe

ions may produce ROS through the Fenton reaction and further contribute to oxidative stress by consuming cellular antioxidants through redox cycling between Fe^{2+} and Fe^{3+}.[53] Divalent ions of cadmium (Cd^{2+}), a transition-metal ion, have also been shown to inhibit the complexes of the ETC (especially complexes II and III) and induce ROS production at the complex III site.[22] Therefore, Co^{2+} may similarly interfere with electron transfer in the ETC and induce ROS production. The decrease in proton leak observed in the presence of Co^{2+} is in agreement with this possibility since inhibition at any position in the ETC would decrease proton pumping activity and thereby decrease the proton-motive force and consequently proton leak.[54,55] Finally, results showed a Co^{2+}-induced decrease in non-mitochondrial oxygen consumption, suggesting that Co^{2+} may also affect NADH oxidase reactions.[18,55,56]

Protein carbonylation is indicative of oxidative stress, and carbonylation of mitochondrial complexes has been reported in heart tissue (complexes I, II, III and the F_0F_1 ATP synthase)[57] as well as in muscle and white adipose tissue (complex I).[58] Furthermore, ROS-induced carbonylation of complex I has been shown to increase ROS production implying a feed-forward control loop amplifying small changes in ROS production and consequent protein carbonylation.[58] Therefore, Co^{2+}-induced ROS production may result in the carbonylation of mitochondrial complexes leading to mitochondrial dysfunction and further ROS production. Interestingly, while the present study showed that Co^{2+}, but not Cr^{3+}, induced oxidative stress, other studies have reported increased oxidative stress in macrophages exposed to Cr^{3+},[9,11,59] albeit to a lesser extent than in macrophages exposed to Co^{2+}.[9,11] This discrepancy in the effects of Cr^{3+} may be explained by differences in methodologies. For example, in the present study (unlike in previous studies[9,11]), nitrogen cavitation was used to lyse cells for the determination of protein carbonyl content because the cells exposed to Co^{2+} or Cr^{3+} exhibited an ion concentration-dependent resistance to lysis by non-ionic detergents (unpublished observation). Furthermore, in the present study the DNPH and

neutralization solutions were prepared in-house because the solutions provided with the OxyBlot® Protein Oxidation Detection Kit (a kit used in previous studies[9,11]) generated overly acidic samples resulting in protein precipitation and SDS-PAGE artifacts (data not shown). Problems with reagents from the OxyBlot® Protein Oxidation Detection Kit have also been reported by others.[34] Notwithstanding, it should be emphasized that the results of the present study are consistent, i.e., Co^{2+}-induced ROS production is associated with an increase in protein carbonylation and mitochondrial dysfunction, whereas Cr^{3+} induced neither ROS production, protein carbonylation nor mitochondrial dysfunction. Finally, the use of different cell models (RAW 264.7 vs. U937, J774A.1, and murine BMDM) cannot presently be excluded as a potential cause of, or contributing factor to, the discrepancy in the effects of Cr^{3+} on oxidative stress.

The observed Co^{2+}-induced decrease in ATP production may lead to the activation of AMP-activated protein kinase (AMPK), resulting in the stimulation of catabolic pathways and inhibition of anabolic pathways to conserve energy.[60] Under these conditions, energy-dependent cellular functions may be negatively affected, especially under scenarios of high energy demand such as those prevailing in macrophages actively involved in immune functions. For example, exposure of macrophages to particles of a Ni- and Cu-based material has been shown to impair phagocytic capacity and mitochondrial function, suggesting a possible causal relationship.[40] In the context of periprosthetic tissues, a Co^{2+}-induced decrease in ATP production could therefore decrease the capacity of macrophages to clear metal wear products. Co^{2+}-induced mitochondrial dysfunction may also prevent repolarization of macrophages from the inflammatory to the anti-inflammatory phenotype.[52] Furthermore, since the energy requirements of the pro- and anti-inflammatory responses of macrophages are primarily met by anaerobic glycolysis and aerobic respiration (i.e., the tricarboxylic acid [TCA] cycle and oxidative phosphorylation), respectively, a Co^{2+}-

induced decrease in ATP production would be expected to primarily decrease the capacity of macrophages to mount an anti-inflammatory response.[61]

CONCLUSION

The present study showed that Co^{2+}, but not Cr^{3+}, induced ROS production and protein carbonylation, suggesting that Co^{2+} induces oxidative stress through an increase in ROS production and possibly through a weakening of antioxidant defenses. Results also showed that Co^{2+} caused mitochondrial dysfunction, including a decrease in oxidative phosphorylation capacity. Overall, these results suggest that mitochondrial dysfunction may contribute to Co^{2+}-induced oxidative stress in macrophages, and thereby to the inflammatory response observed in periprosthetic tissues.

ACKNOWLEDGMENTS

The authors thank Dr. Rodney L. Levine and Nancy B. Wehr for expert advice on the protein carbonyl quantification assay, as well as Corey DeVlugt and Dr. David Patten for expert assistance with the cellular OCR analyses. This work was supported by the Canadian Institutes of Health Research (CIHR), the Canada Research Chairs (CRC) Program, and the Ontario Ministry of Research and Innovation (MRI) (I.C.), as well as by the Natural Sciences and Engineering Research Council of Canada (NSERC) (M-E. H.).

REFERENCES

1. Milošev I. 2012. CoCrMo Alloy for Biomedical Applications. In: Djokić SS editor. Biomedical Applications, Modern Aspects of Electrochemistry: Springer; pp. 1-72.

2. Case CP, Langkamer VG, James C, et al. 1994. Widespread dissemination of metal debris from implants. J Bone Joint Surg Br 76-B:701-712.

3. Catelas I, Jacobs JJ. 2010. Biologic activity of wear particles. Instr Course Lect 59:3-16.

4. Goodman SB, Ma T. 2010. Cellular chemotaxis induced by wear particles from joint replacements. Biomaterials 31:5045-5050.

5. Langton DJ, Jameson SS, Joyce TJ, et al. 2011. Accelerating failure rate of the ASR total hip replacement. J Bone Joint Surg Br 93:1011-1016.

6. Cooper HJ, Della Valle CJ, Berger RA, et al. 2012. Corrosion at the head-neck taper as a cause for adverse local tissue reactions after total hip arthroplasty. J Bone Joint Surg Am 94:1655-1661.

7. Cooper HJ, Urban RM, Wixson RL, et al. 2013. Adverse local tissue reaction arising from corrosion at the femoral neck-body junction in a dual-taper stem with a cobalt-chromium modular neck. J Bone Joint Surg Am 95:865-873.

8. Davidson T, Ke Q, Costa M. 2007. Selected molecular mechanisms of metal toxicity and carcinogenicity. In: Nordberg GF, Fowler BA, Nordberg M editors. Handbook of the toxicology of metals: Elsevier; pp. 79-100.

9. Petit A, Mwale F, Tkaczyk C, et al. 2005. Induction of protein oxidation by cobalt and chromium ions in human U937 macrophages. Biomaterials 26:4416-4422.

10. Luo S, Wehr NB. 2009. Protein carbonylation: avoiding pitfalls in the 2,4-dinitrophenylhydrazine assay. Redox report 14:159-166.

11. Scharf B, Clement CC, Zolla V, et al. 2014. Molecular analysis of chromium and cobalt-related toxicity. Scientific reports 4:5729.

12. Sansone V, Pagani D, Melato M. 2013. The effects on bone cells of metal ions released from orthopaedic implants. A review. Clin Cases Miner Bone Metab 10:34-40.

13. Sies H. 2015. Oxidative stress: a concept in redox biology and medicine. Redox Biology 4:180-183.

14. Sies H, Berndt C, Jones DP. 2017. Oxidative stress. Annu Rev Biochem 86:715-748.

15. Holmström KM, Finkel T. 2014. Cellular mechanisms and physiological consequences of redox-dependent signalling. Nat Rev Mol Cell Biol 15:411-421.

16. Mailloux RJ, McBride SL, Harper M-E. 2013. Unearthing the secrets of mitochondrial ROS and glutathione in bioenergetics. Trends Biochem Sci 38:592-602.

17. Fisher-Wellman H, Lin C-T, Ryan TE, et al. 2015. Pyruvate dehydrogenase complex and nicotinamide nucleotide transhydrogenase constitute an energy-consuming redox circuit. Biochem J 467:271-280.

18. Dixon SJ, Stockwell BR. 2014. The role of iron and reactive oxidative species in cell death. Nat Chem Biol 10:9-17.

19. Valko M, Jomova K, Rhodes CJ, et al. 2016. Redox- and non-redox-metal-induced formation of free radicals and their role in human disease. Arch Toxicol 90:1-37.

20. Foster AW, Osman D, Robinson NJ. 2014. Metal preferences and metallation. J Biol Chem 289:28095-28103.

21. Irving H, Williams RJP. 1953. The stability of transition-metal complexes. J Chem Soc 0:3192-3210.

22. Wang Y, Fang J, Leonard SS, et al. 2004. Cadmium inhibits the electron transfer chain and induces reactive oxygen species. Free Radic Biol Med 36:1434-1443.

23. Chen H, Costa M. 2006. Effect of soluble nickel on cellular energy metabolism in A549 cells. Exp Biol Med 231:1474-1480.

24. Li X, Zhong F. 2014. Nickel induced Interleukin-1ß secretion via the NLRP3-ASC-Caspase 1 pathway. Inflammation 37:457-466.

25. Niki Y, Matsumoto H, Suda Y, et al. 2003. Metal ions induce bone-resorbing cytokine production through the redox pathway in synoviocytes and bone marrow macrophages. Biomaterials 24:1447-1457.

26. Catelas I, Petit A, Zukor DJ, et al. 2003. TNF-α secretion and macrophage mortality induced by cobalt and chromium ions in vitro-Qualitative analysis of apoptosis. Biomaterials 24:383-391.

27. Perino G, Ricciardi BF, Jerabek SA, et al. 2014. Implant based differences in adverse local tissue reaction in failed total hip arthroplasties: a morphological and immunohistochemical study. BMC Clin Pathol 14:1-16.

28. Landgraeber S, Jäger M, Jacobs J, et al. 2014. The pathology of orthopedic implant failure is mediated by innate immune system cytokines. Mediators Inflamm 2014:1-9.

29. Nagy C, Haschemi A. 2015. Time and demand are two critical dimensions of immunometabolism: the process of macrophage activation and the pentose phosphate pathway. Front Immunol 6:1-8.

30. Baskey SJ, Lehoux EA, Catelas I. 2016. Migration of lymphocytes in response to cobalt and chromium ions. J Orthop Res 35:916-924.

31. Wehr NB, Levine RL. 2013. Quantification of protein carbonylation. Methods Mol Biol 965:265-281.

32. Shacter E, Williams JA, Lim M, et al. 1994. Differential susceptibility of plasma proteins to oxidative modification: examination by western blot immunoassay. Free Radic Biol Med 17:429-437.

33. Chen Q, Espey MG, Sun AY, et al. 2007. Ascorbate in pharmacologic concentrations selectively generates ascorbate radical and hydrogen peroxide in extracellular fluid in vivo. PNAS 104:8749-8754.

34. Wang P, Powell SR. 2010. Decreased sensitivity associated with an altered formulation of a commercially available kit for detection of protein carbonyls. Free Radic Biol Med 49:119-121.

35. Devitt BM, Queally JM, Vioreanu M, et al. 2010. Cobalt ions induce chemokine secretion in a variety of systemic cell lines. Acta Orthop 81:756-764.

36. Baskey SJ, Beaulé PE, Lehoux EA, et al. 2014. Simvastatin modulates the release of TNF-α and CC chemokines from macrophages exposed to trivalent chromium ions. J Biomater Tissue Eng 4:981-991.

37. Beidelschies MA, Huang H, McMullen MR, et al. 2008. Stimulation of macrophage TNFα production by orthopaedic wear particles requires activation of the ERK1/2/Egr-1 and NF-κB pathways but is independent of p38 and JNK. J Cell Physiol 217:652-666.

38. Kwon YM, Xia Z, Glyn-Jones S, et al. 2009. Dose-dependent cytotoxicity of clinically relevant cobalt nanoparticles and ions on macrophages in vitro. Biomed Mater 4:025018.

39. Chen W, Li Z, Guo Y, et al. 2015. Wear particles promote reactive oxygen species-mediated inflammation via the nicotinamide adenine dinucleotide phosphate oxidase pathway in macrophages surrounding loosened implants. Cell Physiol Biochem 35:1857-1866.

40. Badding MA, Fix NR, Antonini JM, et al. 2014. A comparison of cytotoxicity and oxidative stress from welding fumes generated with a new nickel-, copper- based consumable versus mild and stainless steel-based welding in RAW 264.7 mouse macrophages. PLoS ONE 9:e101310.

41. Raschke WC, Baird S, Ralph P, et al. 1978. Functional macrophage cell lines transformed by Abelson leukemia virus. Cell 15:261-267.

42. Guentsch A, Beneke A, Swain L, et al. 2016. PHD2 Is a regulator for glycolytic reprogramming in macrophages. Mol Cell Biol 37:1-16.

43. Catelas I, Petit A, Vali H, et al. 2005. Quantitative analysis of macrophage apoptosis vs. necrosis induced by cobalt and chromium ions in vitro. Biomaterials 26:2441-2453.

44. Wang JY, Wicklund BH, Gustilo RB, et al. 1996. Titanium, chromium and cobalt ions modulate the release of bone- associated cytokines by human monocytes/macrophages in vitro. Biomaterials 17:2233-2240.

45. Catelas I, Petit A, Zukor DJ, et al. 2001. Cytotoxic and apoptotic effects of cobalt and chromium ions on J774 macrophages - Implication of caspase-3 in the apoptotic pathway. J Mater Sci Mater Med 12:949-953.

46. Kirkham P. 2007. Oxidative stress and macrophage function: a failure to resolve the inflammatory response. Biochem Soc Trans 35:284-287.

47. Brüne B, Dehne N, Grossmann N, et al. 2013. Redox control of inflammation in macrophages. Antioxid Redox Signal 19:595-637.

48. Gieche J, Mehlhase J, Licht A, et al. 2001. Protein oxidation and proteolysis in RAW264.7 macrophages: effects of PMA activation. Biochim Biophys Acta 1538:321-328.

49. Chen X, Zhong Z, Xu Z, et al. 2010. 2',7'-Dichlorodihydrofluorescein as a fluorescent probe for reactive oxygen species measurement: Forty years of application and controversy. Free Radic Res 44:587-604.

50. Birben E, Sahiner UM, Sackesen C, et al. 2012. Oxidative stress and antioxidant defense. World Allergy Organ J 5:9-19.

51. Christova TY, Gorneva GA, Taxirov SI, et al. 2003. Effect of cisplatin and cobalt chloride on antioxidant enzymes in the livers of Lewis lung carcinoma-bearing mice: protective role of heme oxygenase. Toxicol Lett 138:235-242.

52. Van den Bossche J, Baardman J, Otto NA, et al. 2016. Mitochondrial Dysfunction Prevents Repolarization of Inflammatory Macrophages. Cell Rep 17:684-696.

53. Lemire JA, Harrison JJ, Turner AJ. 2013. Antimicrobial activity of metals: mechanisms, molecular targets and applications. Nat Rev Microbiol 11:371-384.

54. Jastroch M, Divakaruni AS, Mookerjee S, et al. 2010. Mitochondrial proton and electron leaks. Essays Biochem 47:53-67.

55. Brand MD, Nicholls DG. 2011. Assessing mitochondrial dysfunction in cells. Biochem J 435:297-312.

56. Morel F, Doussiere J, Vignais PV. 1991. The superoxide-generating oxidase of phagocytic cells. Physiological, molecular and pathological aspects. Eur J Biochem 201:523-546.

57. Choksia KB, Boylstona WH, Rabeka JP, et al. 2004. Oxidatively damaged proteins of heart mitochondrial electron transport complexes. Biochim Biophys Acta 1688:95-101.

58. Frohnert B, Bernlohr DA. 2012. Protein carbonylation, mitochondrial dysfunction, and insulin resistance. Adv Nutr 4:157-163.

59. Hassoun EA, Stohs DJ. 1995. Chromium-induced production of reactive oxygen species, DNA single-strand breaks, nitric oxide production, and lactate dehydrogenase leakage in J774A.1 cell cultures. J Biochem Toxicol 10:315-321.

60. Kelly B, O'Neill LAJ. 2015. Metabolic reprogramming in macrophages and dendritic cells in innate immunity. Cell Res 25:771-784.

61. Van den Bossche J, O'Neill LA, Menon D. 2017. Macrophage immunometabolism: where are we (going)? Trends Immunol 38:395-406.

FIGURE LEGENDS

Figure 1: Mortality of RAW 264.7 macrophages after a 24-hour exposure to Co^{2+} or Cr^{3+}. Percentage of the total number of cells (viable + dead) that were dead after exposure to (A) Co^{2+} or (B) Cr^{3+}. Total number of cells (viable + dead) after exposure to (C) Co^{2+} or (D) Cr^{3+}. Cells were incubated under cell culture conditions with the indicated concentrations of Co^{2+} or Cr^{3+}. At the end of the incubation, mortality was analyzed by dye-exclusion hemocytometry using trypan blue. The dashed line represents the number of cells 3 hours prior to the start of the 24-hour exposure (see Materials and Methods section). Statistical analysis was performed using a Welch ANOVA followed by Games-Howell post-hoc tests since the homogeneity of variance assumption was unmet, as per Levene's test. An asterisk (*) and double-asterisk (**) indicate a significant difference between a given condition and the negative control, with $p<0.05$ and $p\leq0.001$, respectively. Data are presented as means ± SEM of three independent experiments, each performed with three replicate samples per condition.

Figure 2: Cytosolic reactive oxygen species (ROS) levels in RAW 264.7 macrophages after a 6-hour exposure to (A) Co^{2+} or (B) Cr^{3+}. ROS were assayed using the redox sensitive probe 2′,7′-dichlorodihydrofluorescein diacetate. 2′,7′-Dichlorofluorescein (DCF) concentration, expressed relative to the DCF concentration in the negative control (represented by a dashed line), is directly proportional to the level of cytosolic ROS. Data are presented as means ± SEM of three independent experiments, each performed with 5-6 replicate samples per condition. Statistics as in Figure 1.

Figure 3: Protein carbonyl content in RAW 264.7 macrophages after a 24-hour exposure to Co^{2+} (A-C) or Cr^{3+} (D-F). (A) and (D): Polyacrylamide gels of whole-cell extracts treated with

2,4-dinitrophenylhydrazine, analyzed by SDS-PAGE (3 μg protein per lane), and stained with the protein-binding dye Coomassie Brilliant Blue. (B) and (E): Western blots of protein carbonyls performed with gels ran in parallel to those shown in panels (A) and (D). (C) and (F): Protein carbonyl content (determined by densitometric analysis of the western blots) normalized to protein content (determined by acid-blue staining of the blots) and expressed relative to the negative control (represented by a dashed line). Representative gels and western blots are shown. Data in panels (C) and (F) are presented as means ± SEM of three independent experiments. MW: pre-stained protein molecular weight standards. dMW: 2,4-dinitrophenyl (DNP)-derivatized protein molecular weight standards – the indicated molecular weights are those of the corresponding underivatized proteins. Statistics as in Figure 1.

Figure 4: Cellular oxygen consumption rates (OCR) of RAW 264.7 macrophages following a 6-hour exposure to Co^{2+}: (A) Mitochondrial respiration parameters; (B) Non-mitochondrial oxygen consumption; (C) Proton leak, represented by basal respiration (i.e., mitochondrial respiration that is not coupled to ATP production). OCR (measured using an extracellular flux analyzer) were normalized to protein content (determined using a colorimetric assay). Data are presented as means ± SEM of three independent experiments, each performed with 7-8 replicate samples per condition. Statistics as in Figure 1 except that, since the homogeneity of variance assumption was met for some parameters as per Levene's test, a two-way ANOVA and Tukey-Kramer post-hoc tests were used to analyze these parameters.

Figure 5: Cellular oxygen consumption rates (OCR) of RAW 264.7 macrophages following a 6-hour exposure to Cr^{3+}: (A) Mitochondrial respiration parameters; (B) Non-mitochondrial oxygen consumption; (C) Proton leak, represented by basal respiration (i.e., mitochondrial

respiration that is not coupled to ATP production). OCR (measured using an extracellular flux analyzer) were normalized to protein content (determined using a colorimetric assay). Data are presented as means ± SEM of three independent experiments, each performed with 7-8 replicate samples per condition). Statistics as in Figure 4.

FIGURES

Figure 1

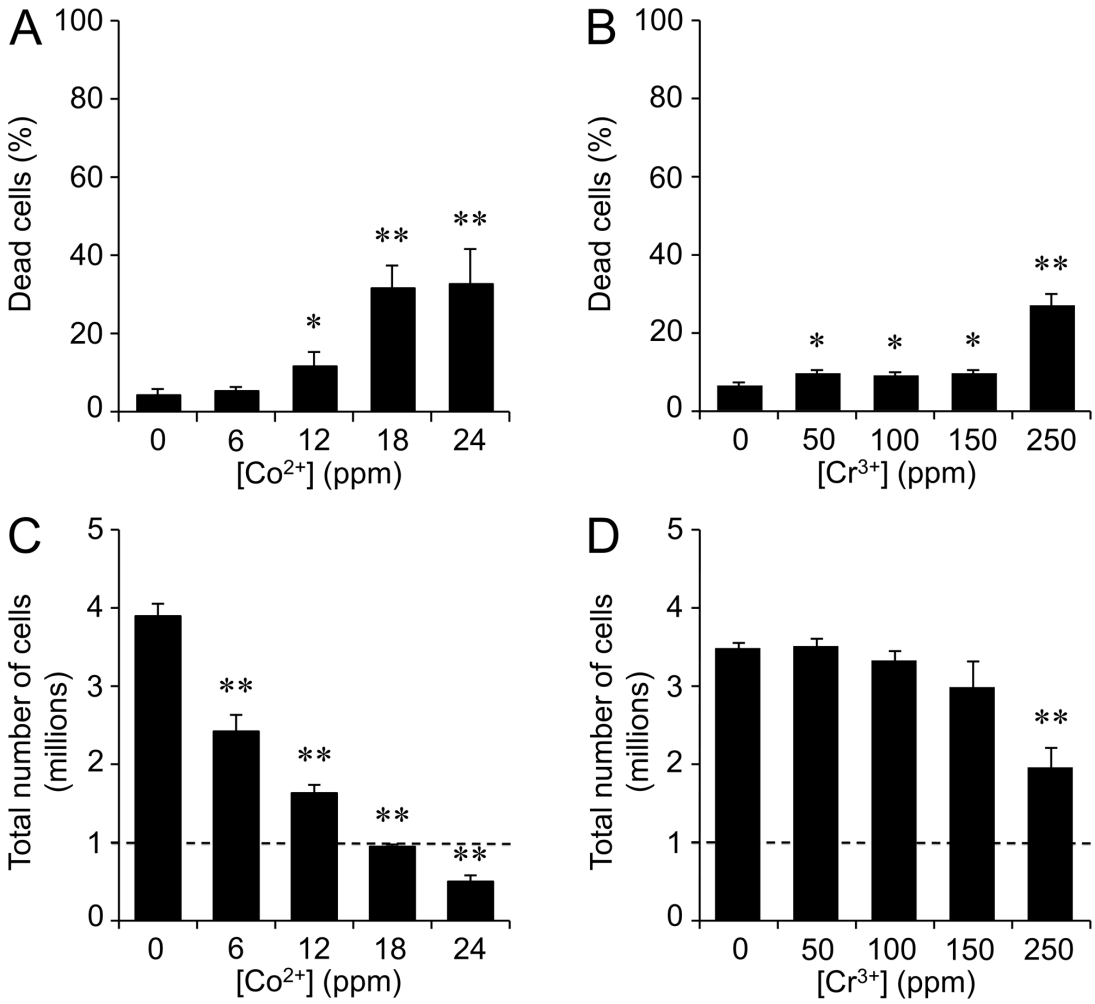

Figure 2

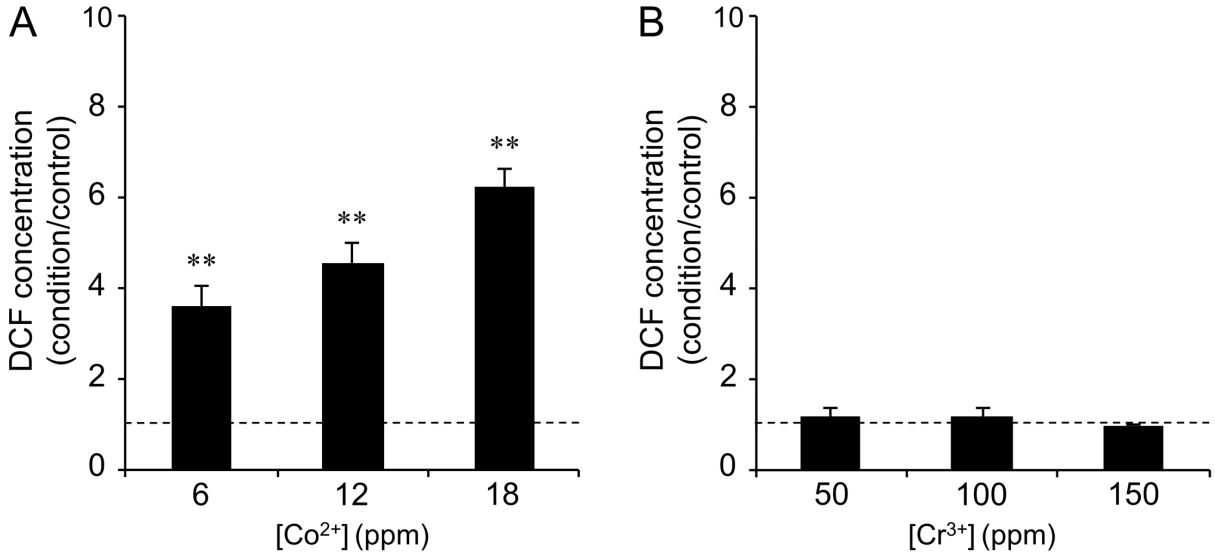
A
B
DCF concentration (condition/control)
10
8
6
4
2
0
**
**
**
6
12
18
[Co2+] (ppm)
50
100
150
[Cr3+] (ppm)

Figure 3

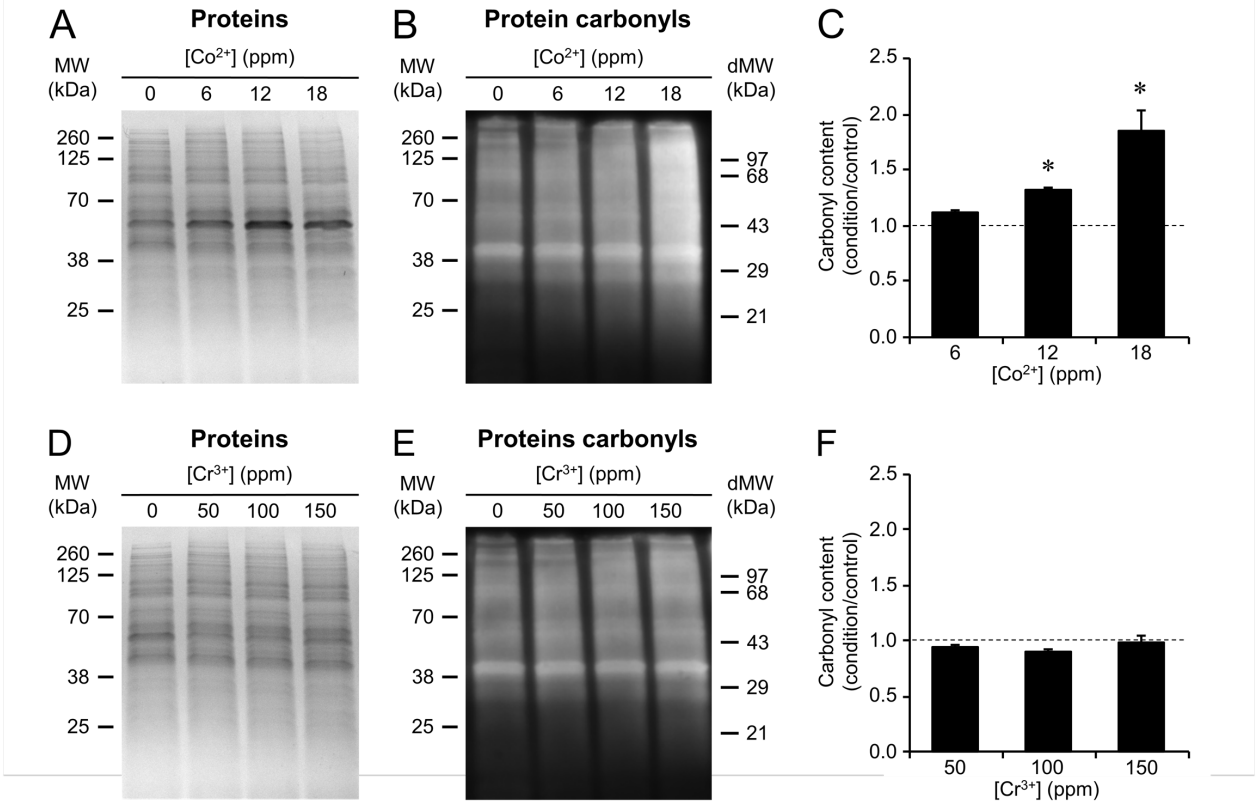
A
Proteins
MW (kDa)
[Co2+] (ppm)
0 6 12 18
260
125
70
38
25
B
Protein carbonyls
MW (kDa)
[Co2+] (ppm)
0 6 12 18
dMW (kDa)
260
125
70
38
25
97
68
43
29
21
C
Carbonyl content (condition/control)
2.5
2.0
1.5
1.0
0.5
0.0
*
*
6 12 18
[Co2+] (ppm)
D
Proteins
MW (kDa)
[Cr3+] (ppm)
0 50 100 150
260
125
70
38
25
E
Proteins carbonyls
MW (kDa)
[Cr3+] (ppm)
0 50 100 150
dMW (kDa)
260
125
70
38
25
97
68
43
29
21
F
Carbonyl content (condition/control)
2.5
2.0
1.5
1.0
0.5
0.0
50 100 150
[Cr3+] (ppm)

Figure 4

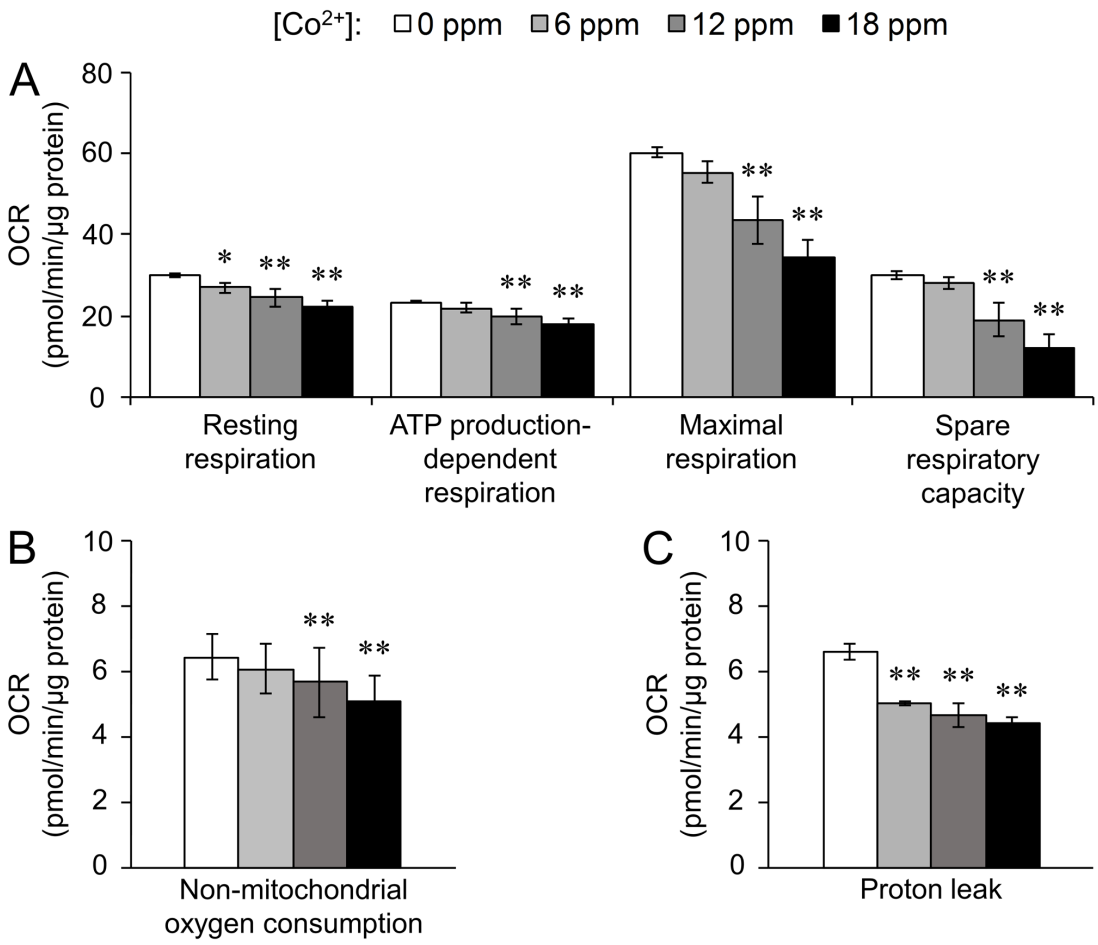
[Co2+]: 0 ppm 6 ppm 12 ppm 18 ppm
A
OCR (pmol/min/µg protein)
80
60
40
20
0
*
**
**
**
**
**
**
**
Resting respiration
ATP production-dependent respiration
Maximal respiration
Spare respiratory capacity
B
OCR (pmol/min/µg protein)
10
8
6
4
2
0
**
**
Non-mitochondrial oxygen consumption
C
OCR (pmol/min/µg protein)
10
8
6
4
2
0
**
**
**
Proton leak

Figure 5

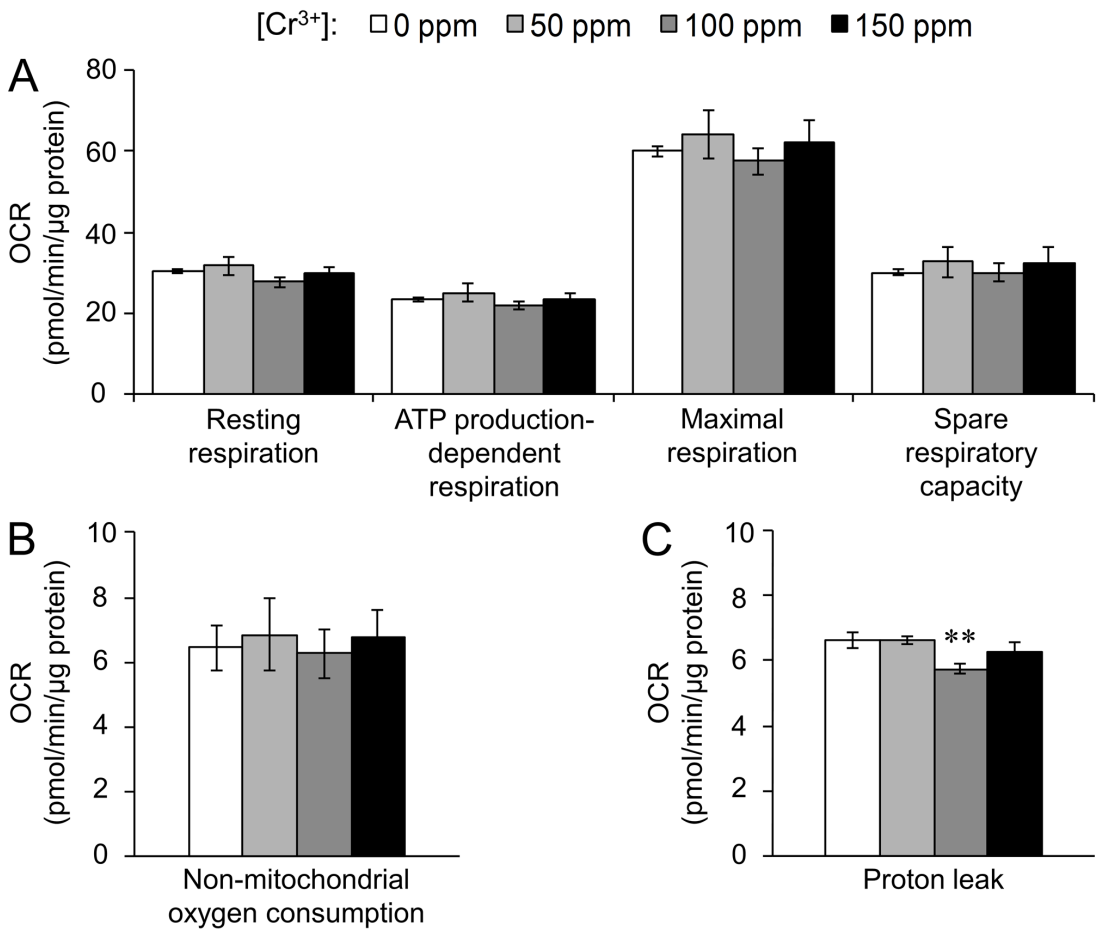
[Cr3+]: 0 ppm 50 ppm 100 ppm 150 ppm
A
OCR (pmol/min/µg protein)
80
60
40
20
0
Resting respiration
ATP production-dependent respiration
Maximal respiration
Spare respiratory capacity
B
OCR (pmol/min/µg protein)
10
8
6
4
2
0
Non-mitochondrial oxygen consumption
C
OCR (pmol/min/µg protein)
10
8
6
4
2
0
**
Proton leak